Environ. Sci. Technol. **2001**, *35,* 2804−2811

Mass Transport Effects on the Kinetics of Nitrobenzene Reduction by Iron Metal

MICHELLE M. SCHERER,*,† KATHLEEN M. JOHNSON,† JOHN C. WESTALL,‡ AND PAUL G. TRATNYEK§

Department of Civil and Environmental Engineering, University of Iowa, Iowa City, Iowa 52242-1527, Department of Chemistry, Oregon State University, 153 Gilbert Hall, Corvallis, Oregon 97331-4003, and Department of Environmental Science and Engineering, Oregon Graduate Institute of Science & Technology, 20000 NW Walker Road, Beaverton, Oregon 97006-8921

To evaluate the importance of external mass transport on the overall rates of contaminant reduction by iron metal (Fe^0), we have compared measured rates of surface reaction for nitrobenzene ($ArNO_2$) to estimated rates of external mass transport in a permeable reactive barrier (PRB). The rate of surface reaction was measured at a polished Fe^0 rotating disk electrode (RDE) in an electrochemical cell, and the rate of mass transport was estimated from a correlation for mass transport in packed-bed reactors. The kinetics of $ArNO_2$ reduction were studied in pH 8.4 borate buffer at a potential below which an oxide film would form. The cathodic current measured in this system was dependent on the electrode rotation rate, and the measured first-order heterogeneous rate coefficient for surface reaction [$k_{rxn} = (1.7 \pm 0.2) \times 10^{-3}$ cm s^{-1}] was about 10 times faster than the first-order mass transport rate coefficient ($k_{mt} \approx 2 \times 10^{-4}$ cm s^{-1}) estimated for PRBs. The similarity between rates of surface reaction and mass transport suggest that it may be important to consider mass transport processes in the design of PRBs for contaminants such as nitroaromatics that are highly reactive with Fe^0.

Introduction

After almost a decade of research and development, it is clear that iron metal (Fe^0) permeable reactive barriers (PRBs) are a cost-effective treatment technology for dissolved chlorinated solvents (*1*). The success of Fe^0 PRBs in treating chlorinated solvents has led many researchers to investigate other classes of reducible contaminants, such as metals (*2*−*5*), radionuclides (*6*, *7*), pesticides (*8*−*10*), azo dyes (*11*, *12*), and explosives (*13*−*18*). Of these classes of compounds, several exhibit rates of reduction that are significantly faster than those observed for most chlorinated solvents. The faster reduction rates observed for these compounds increases the likelihood that mass transport processes affect the overall kinetics of degradation. Despite the increased likelihood of mass transport limitations, most studies have focused on quantifying an observed rate of reduction, with only a few (*19*−*21*) attempting to distinguish between mass transport to the Fe^0 surface and surface processes influencing the reaction rate. Decoupling the observed kinetics into a mass transport contribution and a surface reaction contribution has important practical implications for developing models to optimize the design of PRBs.

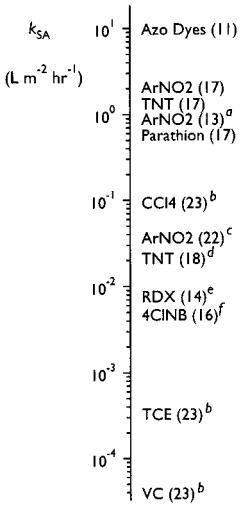

FIGURE 1. Previously reported BET surface area normalized rate coefficients for reduction of selected organic compounds by granular iron metal: (a) calculated from the data in Table 2 of ref *13* and the BET surface area of 0.005 m^2 g^{-1} reported in ref *17* for untreated Fluka Fe^0; (b) average reaction rate coefficients calculated from batch and column data summarized in ref *23*; (c) calculated from the slope of the data given in Figure 4 of ref *22* and a BET surface area of 3.2 m^2 g^{-1}; (d) based on a visual estimate of a 6 h half-life for TNT in the presence 2 g L^{-1} of Fe^0 (see Figure 2 in ref *18*); (e) calculated with a BET surface area of 1.87 m^2 g^{-1} reported by the authors in ref *14*; and (f) based on an Fe^0 surface area concentration of 6300 m^2 L^{-1} calculated for a packed column of 0.9 cm length and 5 cm diameter with a porosity of 0.45 used in ref *16*.

To evaluate whether mass transport effects need to be considered when designing an Fe^0 PRB for the more labile contaminants, we have studied the reduction of nitrobenzene ($ArNO_2$) by Fe^0. The reduction of nitroaromatic compounds, such as nitrobenzene ($ArNO_2$) and 2,4,6-trinitrotoluene (TNT), by Fe^0 has been studied in both batch and column reactors, and they have been found to be highly reactive (*13*, *16*−*18*, *22*). Figure 1 compares surface area normalized rate coefficients (k_{SA}s) reported for these compounds to k_{SA}s reported for other organic contaminants. The average rate coefficient reported for $ArNO_2$ ($k_{SA} \sim 1$ L m^{-2} h^{-1} (*13*, *17*, *22*)) is about 10-fold faster than the average rate coefficient reported for carbon tetrachloride ($k_{SA} = 0.12$ L m^{-2} h^{-1} (*23*)), and more than 3 orders of magnitude faster than trichloroethene ($k_{SA} = 4 \times 10^{-4}$ L m^{-2} h^{-1} (*23*)). The faster reduction rates observed for $ArNO_2$ increases the likelihood that mass transport affects the overall kinetics of degradation.

Other evidence from batch and column experiments also suggest that the observed rates of $ArNO_2$ were influenced by mass transport to the Fe^0 surface. Agrawal and Tratnyek (*17*) concluded that the rate of $ArNO_2$ reduction by Fe^0 was controlled by mass transport because (i) a linear relationship was found between the reaction rate coefficient and the square root of the batch mixing rate (rpm$^{1/2}$), and (ii) no significant substituent effects were found on reduction rates, despite significant differences in one-electron reduction

* Corresponding author phone: (319)335-5654; fax: (319)335-5660; e-mail: michelle-scherer@uiowa.edu.
† University of Iowa.
‡ Oregon State University.
§ Oregon Graduate Institute of Science & Technology.

10.1021/es0016856 CCC: $20.00
© 2001 American Chemical Society
Published on Web 05/25/2001

potentials. To overcome the potential interference of particle abrasion on interpretation of mass transport effects, Devlin and co-workers designed a recirculating batch reactor in which the granular Fe^0 particles were held stationary (*16*). Results from the recirculating batch experiments also showed only a small influence of substituent effects, supporting earlier suggestions that mass transport may be the rate-limiting step. Evidence for mass transport limitations has also been found in columns filled with Fe^0 and sand where equilibrium transport modeling significantly underestimated nitrobenzene break through curves (*22*). A recent study showed that the presence of ultrasound in batch reactors enhanced the rate of $ArNO_2$ reduction by Fe^0 (*13*). The enhancement was attributed to increased rates of mass transport, due to turbulence created by the ultrasound waves, as well as indirect chemical effects, such as surface cleaning and nitric acid production.

The degree to which mass transport determines the overall rate of $ArNO_2$ reduction by Fe^0, however, is difficult to resolve from these studies because of the multitude of indirect effects (both chemical and physical processes) that may occur in batch and column reactors. The granular Fe^0 used in these studies (and others) is covered by a layer of oxide formed from the accumulation of corrosion products at the Fe^0–water interface (*24*). Mass transport through the oxide layer (e.g., by pore diffusion) as well as external diffusion gives rise to three potential kinetic domains: (i) mass transport limited kinetics, where $ArNO_2$ diffuses to the surface more slowly than it reacts at the surface, (ii) reaction limited kinetics, where $ArNO_2$ reacts at the surface more slowly than it diffuses to the surface, and (iii) intermediate kinetics, where mass transport and surface reaction occur on similar time-scales. Behavior typical of mass transport limited kinetics (e.g., faster rates with increased mixing intensity) may occur from indirect physical effects such as abrasion of the oxide layer (*16*, *19*), making it difficult to confirm whether the observed kinetics are measuring diffusion rates, reaction rates, or a combination of both.

To overcome these difficulties, we have developed an alternative experimental approach that avoids the formation of an oxide layer and separates external mass transport rates from surface reaction rates (*21*). The experimental design consists of an electrochemical cell with an oxide-free Fe^0 rotating disk electrode (RDE). Since no oxide forms on the Fe^0 RDE (in the potential range of active corrosion), pore diffusion is eliminated as a potential mass transport process. These conditions create an Fe^0–$ArNO_2$–H_2O system where external mass transport and surface reaction (which includes sorption processes, such as surface attachment and rearrangement, as well as electron transfer) are the dominant processes. The controlled hydrodynamics of an RDE are well understood (*25*, *26*) and can be used to quantify the external mass transport and surface reaction contributions to the observed reduction rate. In this study, the RDE is used to isolate mass transport rates from the rate of $ArNO_2$ reduction by Fe^0.

The specific objectives of this study were (i) to measure a first-order heterogeneous reaction rate coefficient (k_{rxn}) for the reduction of $ArNO_2$ by Fe^0, (ii) to estimate a first-order mass transport coefficient (k_{mt}) for the transport of $ArNO_2$ in PRBs, and (iii) to evaluate the significance of mass transport effects on removal rates of highly reactive compounds in Fe^0 PRBs. For this study, we have focused on $ArNO_2$ as a representative nitroaromatic compound, high-purity iron in the absence of corrosion products, and pH 8.4 borate buffer.

Background

Electrochemical Kinetic Model. We have previously presented a conceptual model of carbon tetrachloride (CCl_4) reduction at an Fe^0 RDE that includes a two-step reaction sequence consisting of diffusion through the hypothetical stagnant layer formed at the Fe^0 RDE–water interface and reaction at the Fe^0 RDE surface. Based on this model, we have shown how to derive a first-order heterogeneous reaction rate coefficient (k_{rxn}) from experimental current density versus voltage (*j*-E) data (*21*). Several variations on this derivation have been published in more recent studies dealing with other electrochemical aspects of contaminant degradation using Fe^0 (*27*–*30*). The number of intermediates and products obtained by the reduction of $ArNO_2$ by Fe^0, however, requires a more complex model with multiple steps to account for the reaction and diffusion of each intermediate to and from the electrode (*17*).

Chemical Reactions. The complete reduction of $ArNO_2$ to aniline ($ArNH_2$) by Fe^0 involves six electrons and can be written as

$$ArNO_2 + 3Fe^0 + 6H^+ \rightarrow ArNH_2 + 3Fe^{2+} + 2H_2O \quad (1)$$

Equation 1 represents the sum of several two-electron half-reactions: the oxidation of Fe^0

$$Fe^0 \rightarrow Fe^{2+} + 2e^- \quad (2)$$

and the sequential reduction of $ArNO_2$ to nitrosobenzene (ArNO), phenyl hydroxylamine (ArNHOH), and aniline

$$ArNO_2 + 2H^+ + 2e^- \rightarrow ArNO + H_2O \quad (3)$$

$$ArNO + 2H^+ + 2e^- \rightarrow ArNHOH \quad (4)$$

$$ArNHOH + 2H^+ + 2e^- \rightarrow ArNH_2 + H_2O \quad (5)$$

In addition to the reduction of $ArNO_2$ and oxidation of Fe^0, the reduction of water (by Fe^0) also occurs and must be considered in evaluating current densities at an Fe^0 electrode:

$$2H_2O + 2e^- \rightarrow H_2(g) + 2OH^- \quad (6)$$

The net current density (j_{net}, A m^{-2}) observed at an Fe^0 RDE in the presence of dissolved $ArNO_2$ is the sum of the partial current densities (j_x, A m^{-2}) for each of the reactions described in eqs 2–6

$$j_{net} = j_{Fe} + j_{NB} + j_{NO} + j_{NHOH} + j_H \quad (7)$$

where Fe, NB, NO, NHOH, and H refer to the overall partial current densities associated with each reaction, respectively. It will be shown, however, that the current from the reduction of ArNO and ArNHOH ($j_{NO} + j_{NHOH}$) are small compared to that from the reduction of $ArNO_2$ (j_{NB}). The net current density can therefore be approximated by

$$j_{net} = j_{Fe} + j_{NB} + j_H \quad (8)$$

For the case of reaction limited kinetics (i.e., negligible mass transport effects), the partial current density for the reduction and oxidation of species *x*, respectively, can be approximated by a form of the Tafel eq (*31*)

$$j_{x,rxn} = -nFk_x^0 C_x^s \exp\{-(E - E_x^{eq})/b_x\} \quad (9)$$

$$j_{x,rxn} = nFk_x^0 C_x^s \exp\{(E - E_x^{eq})/b_x\} \quad (10)$$

where *n* is the number of electrons in the reaction, *F* is Faraday's constant (96485 C mol^{-1}), k_x^0 (for reaction *x*) is the standard heterogeneous rate coefficient, C_x^s is the aqueous concentration of species *x* at the surface, *E* is the electrode

potential (relative to a specified reference electrode), E_x^{eq} is the equilibrium potential for the half reaction or an approximation thereof, and b_x is an empirical parameter known as the Tafel slope.

A first-order heterogeneous reaction rate coefficient for a reduction process can be calculated from

$$k_{x,rxn} = k_x^{\,0}\exp\{-(E - E_x^{\,eq})/b_x\} \qquad (11)$$

The value of $k_{x,rxn}$ that is relevant for Fe^0 surfaces not under potential control, as in most groundwater remediation operations, can be calculated from eq 11 by setting the applied potential (E) equal to the corrosion potential (E_{corr}). The corrosion potential can be found (for a given concentration) by setting the net current density, j_{net}, equal to zero in eq 8.

Mass Transport. For the case of mass transport limited kinetics, the partial current density for the reduction of species x at an RDE can be approximated by the Levich eq (*31*)

$$j_{x,mt} = 0.620nFD_x^{\,2/3}\,\omega^{1/2}\,\nu^{-1/6}(C_x^{\,b} - C_x^{\,s}) \qquad (12)$$

in which j_x is the current density at the electrode, D_x is the molecular diffusion coefficient, ν is the kinematic viscosity of the electrolyte, ω is the angular velocity of the rotating disk ($\omega = 2\pi f$, where f = rotation rate in s^{-1}), and C^s and C^b are the aqueous concentrations of species x at the surface and in the bulk solution.

Intermediate Kinetics. For the case of intermediate kinetics, where both chemical reaction and mass transport processes influence the reaction rate, the overall partial current density for the reduction of species x (for a first-order irreversible chemical reaction under steady-state conditions) is

$$j_x = j_{rxn,x}\,j_{mt,x}/(j_{rxn,x} + j_{mt,x}) \qquad (13)$$

Experimental Section

Electrochemical Experiments. Experiments were carried out in a custom three-electrode glass cell, which has been described previously (*21*). The cell consisted of an Fe^0 RDE working electrode (geometric surface area = 0.071 cm^2), a double-junction saturated calomel reference electrode, a Pt mesh counter electrode, and a pH 8.4 borate buffer electrolyte (0.11 M). Pretreatment of the electrode has been described previously (*21*). Following pretreatment, $ArNO_2$ was introduced into the cell by injection of a known volume of deaerated aqueous stock solution through a septum. Linear sweep voltammograms (LSVs) were obtained with and without $ArNO_2$ using a potentiostat (EG&G Model 283A). All LSVs were obtained by scanning anodically at a scan rate of 0.2 mV s^{-1}. Initial experiments at slower scan rates verified that 0.2 mV s^{-1} provided sufficient time for steady-state conditions to develop. Potentials are reported relative to the standard hydrogen electrode (SHE), and currents are reported in accord with IUPAC convention (anodic current is positive and cathodic current is negative). Coulometry was used to assess the current efficiency, that is, the fraction of the current passed that results in the transformation of $ArNO_2$. The concentration of $ArNO_2$ and its reaction products were determined by HPLC with UV absorbance detection. Details of the analytical method have been described previously (*17*).

Results and Discussion

Coulometry. To confirm that the observed current densities are due to the reduction of $ArNO_2$ by the Fe^0 RDE, the concentrations of reaction products in the cell solution were compared to those expected from the total cathodic charge passed. From Faraday's law, the amount of product (N, mol) is related to the amount of charge (q, C) by $N = q/nF$. For nitrobenzene reduction, however, the comparison must take into account the formation of the nitroso and hydroxylamine intermediates as well as the final amine product. Therefore

$$q_{tot} = (2N_{NO} + 4N_{NHOH} + 6N_{NH_2}) \times F \qquad (14)$$

where 2, 4, and 6 represent the number of electrons transferred to form the product from the reduction of $ArNO_2$. A comparison of the products measured by HPLC and the total charge provides an estimate of the current efficiency. Approximately 72% of the total cathodic charge (q_{tot} = 2.08 C) could be accounted for by nitrosobenzene (60%) and aniline (12%) in a long-term electrolysis experiment (26 h with $E_{appl} = -0.60$ V). An unidentified peak at a retention time of 4.4 min (cf. ~5.4 min for aniline, 8.6 min for nitrobenzene, and 9.1 min for nitrosobenzene) most likely corresponds to the hydroxylamine intermediate for which a standard was not available (*17*, *32*, *33*), and this could contribute to the 28% of measured charge that is not accounted for by the formation of identified projects. To check if any of this 28% may be due to products sorbed to the Fe^0 surface (which has been shown to occur with granular Fe^0 (*16*)), we extracted products from the Fe^0 surface with hexane. No products were detected in the hexane indicating that sorption of reaction products on the Fe^0 electrode is not significant.

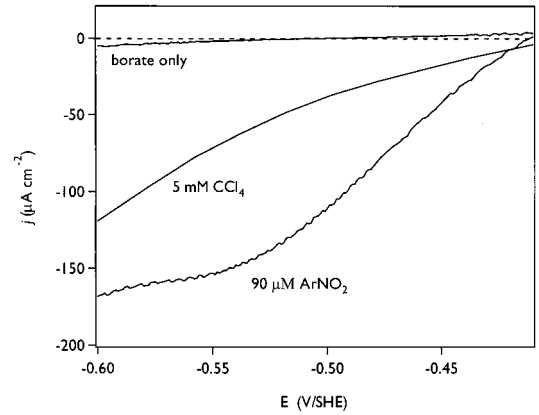

FIGURE 2. Effect of CCl_4 and $ArNO_2$ concentration on steady-state *j-E* curves at an oxide-free Fe^0 RDE rotating at 2500 rpm.

Linear Sweep Voltammetry with an Fe^0 RDE. LSVs with the Fe^0 RDE in aqueous borate buffer and in aqueous borate buffer with $ArNO_2$ are shown in Figure 2. For comparison to our previous work (*21*), a voltammogram for CCl_4 is also shown. In the potential region where the passive film does not form (i.e., $E < -400$ mV), the presence of both CCl_4 and $ArNO_2$ result in an increase in cathodic current density compared to that observed in borate buffer alone. Although the increase in current density appears to be of a similar magnitude for both compounds, it is important to note that the concentration of CCl_4 used (5 mM) is more than 50 times greater than that of $ArNO_2$ (90 μM). The primary product observed for both CCl_4 and $ArNO_2$ ($CHCl_3$ and ArNO, respectively) corresponds to two electrons transferred to form the product (i.e., $n = 2$). The observed current densities are therefore directly comparable, and the similarity for such different concentrations suggests that the rate coefficient for the reduction of $ArNO_2$ at an Fe^0 RDE is considerably larger than the rate coefficient for CCl_4 reduction. This observation is consistent with reduction rates observed in batch experiments with granular Fe^0 metal, where the average surface area normalized rate coefficient reported for $ArNO_2$ ($k_{SA} \sim 1$ L m^{-2} h^{-1}) (*13*, *17*, *22*) is about 10 times greater than the average value reported for CCl_4 ($k_{SA} = 0.12$ L m^{-2} h^{-1}) (*23*).

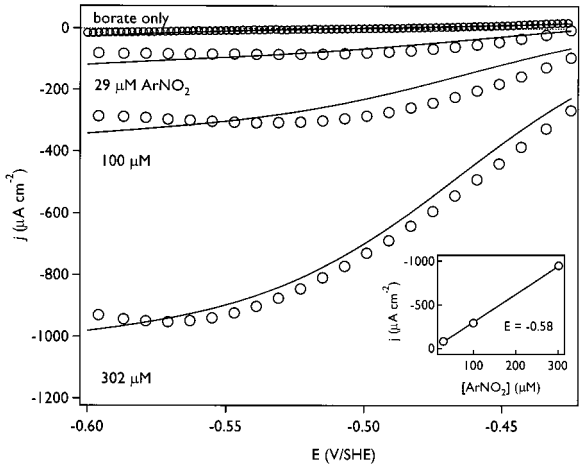

FIGURE 3. Effect of $ArNO_2$ concentration on steady-state *j-E* curves at an oxide-free Fe^0 RDE rotating at 7400 rpm. Only a representative number of data points are shown to distinguish between the model and the data. The kinetics are modeled with eq 15, and the local parameters are given in Table 1. Inset: Current densities at $E = -0.58$ V as a function of $ArNO_2$ concentration.

In addition to differences in rates of reduction, there are notable differences in the shape of the LSVs for $ArNO_2$ and CCl_4. An exponential *j-E* relationship is observed for CCl_4 that is indicative of Tafel behavior (eq 9), whereas the *j-E* relationship for $ArNO_2$ is initially linear (at low overpotentials) and then approaches a plateau in current density at more negative potentials (high overpotentials). The Tafel behavior observed for CCl_4 is consistent with a reaction that is not affected by mass transport (i.e., the surface CCl_4 concentration does not differ appreciably from the bulk concentration) (*21*). On the other hand, the leveling-off behavior observed for $ArNO_2$ suggests that $ArNO_2$ is being reduced as fast as it can be transported to the electrode surface.

LSVs at different concentrations of $ArNO_2$ (29−302 μM) are shown in Figure 3. Higher $ArNO_2$ concentrations result in larger current densities over the entire range of applied potentials. Similar to Figure 2, a plateau in current densities occurs at more negative potentials. The proportional increase in the plateau current density with $ArNO_2$ concentration (shown in Figure 3 inset) confirms that $ArNO_2$ reduction at the Fe^0 RDE is a first-order process ($R^2 > 0.99$).

Effect of Electrode Rotation Rate. LSVs measured at different electrode rotation rates (in the presence of $ArNO_2$) are shown in Figure 4A. In our previous work (*21*), rotation rate had little effect on the reduction of CCl_4 at an Fe^0 RDE. In contrast to the Fe^0−CCl_4−H_2O system, current densities due to $ArNO_2$ reduction increase as the rotation rate is increased, indicating that mass transport to the surface is influencing the overall reaction rate. The influence of mass transport on the rate of $ArNO_2$ reduction by the Fe^0 RDE is consistent with the similarity in reduction rates observed for a series of monosubstituted nitroaromatic compounds by granular Fe^0 (*16, 17*).

To quantitate the degree of mass transport influence on $ArNO_2$ reduction by the Fe^0 RDE, the steady-state current densities in Figure 4A are replotted against the square root of rotation rate in Figure 4B. For a reaction that is completely mass transport limited, current should vary linearly with the square root of electrode rotation rate ($rpm^{1/2}$) and have a *y*-intercept of zero (eq 12). For reduction of $ArNO_2$ at the Fe^0 RDE, a linear relationship is observed between current density and square root of rotation rate for electrode rotation rates below 4900 rpm. At higher rotation rates (rpm > 4900), the deviation from a straight line indicates that $ArNO_2$ is being transported to the surface as fast as it can react. For potentials

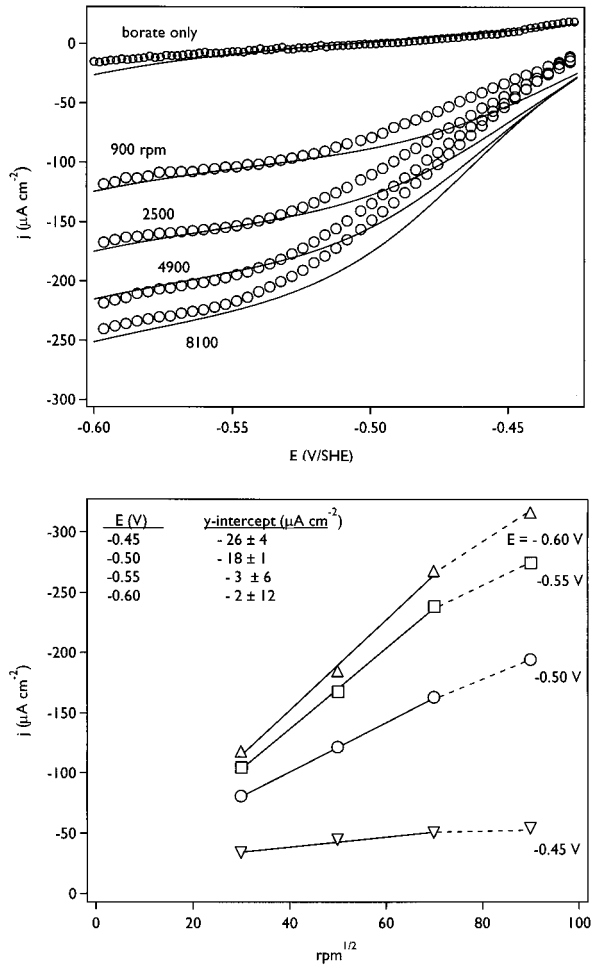

FIGURE 4. (A) Effect of electrode rotation rate on steady-state *j-E* curves at an oxide-free Fe^0 RDE in the presence of ~90 uM $ArNO_2$. Only a representative number of data points are shown to distinguish between the model and the data. The kinetics are modeled with eq 15 and the local parameters given in Table 1. (B) Effect of rotation rate on $ArNO_2$ current densities at an Fe^0 RDE. Steady-state current densities at $E = -0.60$ V for 103 μM $ArNO_2$ (triangles), $E = -0.55$ V for 90 μM $ArNO_2$ (squares), $E = -0.50$V for 82 μM $ArNO_2$ (circles), and $E = -0.45$ V for 76 μM $ArNO_2$ (inverted triangles). Solid lines represent linear regression of data collected at lower rotation rates, whereas the dashed lines connect the two data points at higher rotation rates.

less than −0.55 V, extrapolation of the linear regions of Figure 4B to rpm = 0 results in *y*-intercepts close to the origin (−2 ± 12 and −3 ± 6 μA cm^{-2}). This region corresponds to high overpotentials, where $ArNO_2$ reacts faster than it can be transported to the surface (i.e., where the current density plateaus in Figure 4A). At more positive potentials ($E > -0.55$ V), the values of the *y*-intercepts are significantly different from zero (−18 ± 1 and −26 ± 4 μA cm^{-2}), corresponding to the foot of the waves in Figure 4A, where both reaction and mass transport to the surface are influencing the overall reaction rate. These deviations from a completely mass transport limited behavior (i.e., a straight line that intersects the origin) suggest that the reaction kinetics of $ArNO_2$ at an Fe^0 RDE are influenced by both surface reaction *and* mass transport (i.e., an intermediate kinetic domain) over the range of conditions studied.

Chemical Reaction Kinetics. Since the reduction of $ArNO_2$ in our system occurs under an intermediate kinetic domain where mass transport effects are significant, the surface reaction kinetics cannot be quantified directly from the LSVs presented in Figures 3 and 4A (as was previously done in the

TABLE 1. Electrochemical Kinetic Parameters for $Fe^0-ArNO_2-H_2O$ System[a]

LSV	k^0 (cm s^{-1})	b (V)	D (cm^2 s^{-1})	no. of data points
local Figure 3 f(C) LSVs	4.0×10^{-17}	3.7×10^{-2}	9.6×10^{-6}	225
local Figure 4 f(rpm) LSVs	7.8×10^{-22}	2.8×10^{-2}	7.9×10^{-6}	701
global Figures 3 and 4	1.2×10^{-17}	3.6×10^{-2}	9.0×10^{-6}	926

[a] Estimated with $n = 2$ and $E_{eq}(W) = 0.78$ V for $ArNO_2$ reduction to ArNO (*46*) and eqs 9, 12, and 15. The partial current densities for Fe^0 oxidation and water reduction were estimated with parameters previously determined for the Fe^0-CCl_4-H_2O system (Fe: $j_{Fe}^0 = 1.5 \times 10^{-6}$ A cm^{-2}, $b_{Fe} = 0.077$ V, and $E_{Fe}eq = -0.620$ V; water: $j_H^0 = 5.5 \times 10^{-6}$ A cm^{-2}, $b_H = 0.061$ V, and $E_H eq = -0.500$ V) (*21*)).

Fe^0-CCl_4-H_2O system). To decouple the overall kinetics into separate parameters for chemical reaction (k^o_{NB}, b_{NB}) and mass transport (D_{NB}), we have applied an electrochemical kinetic model to characterize the reaction kinetics of the $Fe^0-ArNO_2-H_2O$ system. By combining eqs 8 and 13, an expression for the net current density (j_{net}) can be derived for the simplified case where the reduction of $ArNO_2$ to ArNO is the dominant reaction:

$$j_{net} = j_{Fe} + j_H + \frac{j_{NB,rxn} j_{NB,mt}}{j_{NB,rxn} + j_{NB,mt}} \qquad (15)$$

A combination of eq 15, the Tafel equations (eqs 9 and 10), and the Levich equation (eq 12) results in a multivariate model where the observed current density, j_{net}, can be expressed in terms of applied potential (E), electrode rotation rate (rpm), and bulk concentration of $ArNO_2$ (C^b).

From the measured steady-state j-E curves in Figures 3 and 4A, values of the parameters k^o_{NB}, b_{NB}, and D_{NB} for $ArNO_2$ reduction were determined by nonlinear least squares parameter adjustment with the multivariate model (eqs 9, 10, 12, and 15). The model was fit separately to each data set in Figures 3 and 4 and globally to the combined data set. The parameters derived from the local and global fitting can be compared in Table 1. The currents estimated from the model with the local parameters are shown by the solid lines in Figures 3 and 4A. A graphical and statistical comparison of experimentally measured currents with estimated currents from the model (with the global parameters given in Table 1) is provided in the Supporting Information.

The surface reaction parameters derived from this model (k^o_{NB} and b_{NB}) provide a basis for estimating a first-order heterogeneous rate coefficient for the reduction of $ArNO_2$ by Fe^0 (under no applied potential). The current due to $ArNO_2$ reduction (for a given concentration) can be estimated from the corrosion potential found from eq 8 (by setting $j_{net} = 0$) and the global parameters given in Table 1. A plot of current (i.e., "rate") versus $ArNO_2$ concentration gives a line with a slope of $nFk_{NB,rxn}$ (data not shown, $R^2 = 0.94$). From this slope, we can calculate a surface area normalized heterogeneous rate coefficient due to surface reaction. The value obtained is $k_{NB,rxn} = (1.7 \pm 0.2) \times 10^{-3}$ cm s^{-1} (63 ± 8 L m^{-2} h^{-1}). This value is about 50 times greater than the average reduction rate coefficient determined from previously reported batch and column experiments performed with granular iron ($k_{SA} \approx 1$ L m^{-2} h^{-1}) (*13, 17, 22*). A greater reduction rate at the Fe^0 RDE is expected due to the slower rate of mass transport in batch experiments (due to less mixing intensity) and the absence of an oxide film that is typically present in conventional experiments and field-scale PRBs.

Mass Transport Kinetics. The mass transport parameter derived from our model is the diffusion coefficient for $ArNO_2$ (D_{NB}). The value of D_{NB} ranges from (7.9 to 9.6) $\times 10^{-6}$ cm^2 s^{-1} for the local and global fitting methods (Table 1). These values are consistent with those estimated by Devlin and co-workers (*16*) ($D_{NB} = 8.2 \times 10^{-6}$ cm^2 s^{-1}) and Agrawal and Tratnyek (*17*) ($D_{NB} = 6.8 \times 10^{-6}$ cm^2 s^{-1}) using the method developed by Wilke and Chang (*34*). The diffusion coefficient is a fundamental parameter that is independent of reactor geometry and flow rates. The actual rate of mass transport, however, is strongly influenced by both of these and (for comparison purposes) can be expressed as a single lumped parameter known as the mass transport coefficient (k_{mt}) (*35*). Given the significant differences in geometry and flow, mass transport rates in a PRB are likely to be quite different from those at an oxide-free Fe^0 RDE. To assess the likelihood of mass transport effects in PRBs, we need to compare mass transport rates relevant to a PRB to the surface reaction rate determined from the Fe^0 RDE experiments.

As a first approximation, mass transport coefficients relevant to a PRB were estimated from empirical correlations developed to describe mass transport in packed-bed reactors. These correlations typically take the form of the Sherwood number ($Sh = k_{mt}d/D$) as the dependent variable and both the Reynolds number ($Re = ud/\nu$) and Schmidt number ($Sc = \nu/D$) as independent variables (*35, 36*) (d is the particle diameter and u is the fluid velocity). A correlation developed for packed bed reactors with hydrodynamic conditions corresponding to low Reynolds numbers (*37*) has been used previously by Arnold and co-workers (*19*) to estimate mass transport coefficients in a hypothetical PRB packed with granular zinc metal:

$$Sh = k_{mt}d/D = 1.09\epsilon^{-2/3}\, Re^{1/3}\, Sc^{1/3} \qquad (16)$$

The correlation predicts that mass transport rates in a packed-bed reactor will decrease with particle size diameter (d) and increase with fluid velocity (u). Thus, the mass transport coefficient in a PRB will be dependent on the velocity of the groundwater and size of the Fe^0 grains. Assuming an ideal spherical geometry, granular Fe^0 used in Fe^0 PRBs (e.g., Connelly or Peerless) can be characterized with particle diameters (d) ranging from 0.5 to 2 mm (35 to 20 mesh size). For a groundwater velocity of 0.3 m dy^{-1}(1 ft dy^{-1}), an Fe^0 particle diameter of 1.0 mm, a porosity (ϵ) of 0.65 (38), and a $ArNO_2$ diffusion coefficient of 9.0×10^{-6} cm^2 s^{-1}, we estimate a mass transport coefficient of 2.3×10^{-4} cm s^{-1} using eq 16. Given accurate input parameters, the accuracy of these solid–liquid mass transport correlations is estimated to be about $\pm 10\%$ (35). Greater uncertainty, however, may be introduced by equating flow in a PRB with flow in a packed-bed reactor.

Implications for PRB Design. Mass transport coefficients estimated with the packed-bed correlation given in eq 16 can be compared with the measured rate coefficient for reaction to determine whether the overall rate of contaminant removal is limited by mass transport. Using the estimated k_{mt} of 2.3×10^{-4} cm s^{-1} and the measured k_{rxn} of 1.7×10^{-3} cm s^{-1}, we calculated an external effectiveness factor (Ω) close to zero indicating that external resistance to mass transfer is significant (*39*). Another dimensionless number often used to quantify the relative rates of reaction and mass transport is the second Damköhler number ($D_{a2} = k_{rxn} L^2/D$) (*35, 40*). For $D_{a2} \ll 1$ (i.e., surface reaction is much slower than mass transport), the removal process is controlled by the rate of surface reaction, and there is little that can be done in terms of the hydraulic design of a PRB to enhance the removal rates. On the other hand, for a process influenced by mass transport (i.e., $D_{a2} \gg 1$), increasing the groundwater velocity through the PRB will increase k_{mt}, and hence, increase $k_{overall}$ (since by analogy to eq 13, $k_{overall} = k_{mt}k_{rxn}/[k_{mt} + k_{rxn}]$).

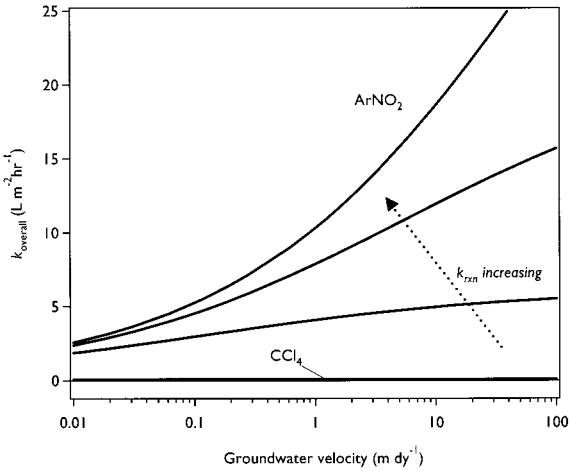

FIGURE 5. Effect of groundwater velocity on overall rate coefficients for reduction of organic compounds by Fe^0. $k_{overall}$ was calculated from $k_{overall} = k_{mt}k_{rxn}/(k_{mt} + k_{rxn})$ with geometric surface area normalized reaction rate coefficients measured with the Fe^0 RDE ($k_{rxn,NB} = 1.7 \times 10^{-3}$ cm s^{-1} and $k_{rxn,CCl4} = 2.3 \times 10^{-5}$ cm s^{-1} (*21*)) and mass transport coefficients estimated with the packed-bed correlation given in eq 16 ($d = 1.0$ mm, $\nu = 0.01$ cm^2 s^{-1}, $\epsilon = 0.65$, and $D_{NB} = 9.0 \times 10^{-6}$ cm s^{-1}).

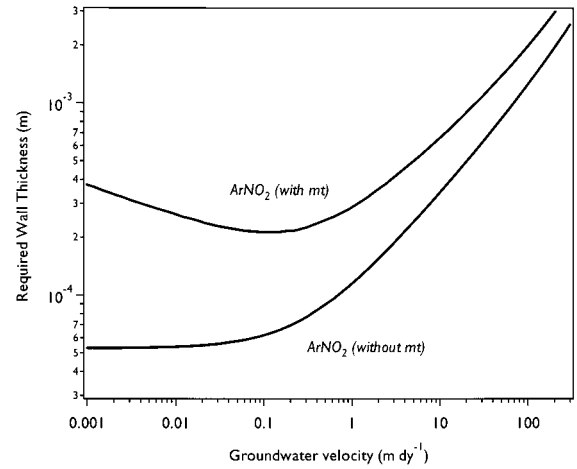

FIGURE 6. Effect of mass transport on preliminary barrier width design curves for 1000-fold removal of $ArNO_2$ as a function of groundwater velocity. Curves are based on steady-state reactive transport model (*43*−*45*) modified to include $k_{overall}$ as a function of groundwater velocity. $k_{overall}$ values were calculated with the parameters given in Figure 5.

Figure 5 shows the effect of groundwater velocity on $k_{overall}$ for a series of compounds with a range of surface reaction rates. For slower reactions (such as the reduction of chlorinated aliphatics by Fe^0), the surface reaction is much slower than mass transport (i.e., $D_{a2} \ll 1$), and $k_{overall}$ is independent of groundwater velocity. For faster reactions, such as those observed for $ArNO_2$, the rate of mass transport is slower than the rate of surface reaction and a velocity dependence arises. A similar dependence of overall rates on groundwater velocity has been depicted for the reduction of chlorinated ethanes in a hypothetical PRB of zinc metal (*19*).

The increase in $k_{overall}$ with faster groundwater velocities accounts for rate-limited degradation caused by solute mass transport processes that are slower than the surface reaction (i.e., $D_{a2} > 1$). A second cause of transport limited degradation occurs when hydraulic residence times (τ_{RH}) are slower than mass transport times. The ratio of mass transport times to system hydraulic residence time is quantified by the first Damköhler number ($D_{a1} = k_{overall}L/u$). As groundwater velocities are increased, low values of D_{a1} can occur which result in longer times for a PRB to reach steady-state conditions (*41*, *42*). Thus, as groundwater velocities are increased, there are two transport related changes that may affect PRB performance: (i) a faster mass transport time, which would result in a faster overall removal rate and improved PRB performance and (ii) a shorter residence time, which would hinder PRB performance.

To evaluate the influence of these two opposing processes, we modified a one-dimensional steady-state transport model (*43*), which has previously been used to estimate barrier widths for a series of chlorinated aliphatic compounds (*44*), to account for solute mass transport limitations. The resulting barrier width design curves for a 1000-fold reduction in $ArNO_2$ are shown in Figure 6 with and without mass transport effects incorporated into the model. Incorporating mass transport effects results in wider barriers over a range of groundwater velocities as well as an optimum velocity for $ArNO_2$ removal ($u \approx 0.2$ m dy^{-1}). The increase in required wall thickness observed at lower groundwater velocities is a result of decreasing the overall rate of reduction (since k_{mt} gets smaller as u decreases), whereas the increase in required wall thickness observed at higher groundwater velocities is a result of shorter residence times. The barrier widths predicted for $ArNO_2$, however, are significantly smaller than those predicted for chlorinated solvents (*44*) (because of the faster rate of $ArNO_2$ reduction by Fe^0) and are physically unrealistic. These results suggest that, at realistic wall widths, mass transport limitations due to short residence times would be unlikely for the reduction of highly reactive compounds (such as $ArNO_2$ and TNT) in Fe^0 PRBs. Mass transfer effects due to solute mass transport processes, however, should be considered, as certain design strategies that increase the groundwater velocity (e.g., funnel and gate systems) may lead to more efficient use of the reactive media.

Acknowledgments

We would like to acknowledge the donors of the Petroleum Research Fund, administered by the ACS for partial support of this research (34640-G5 and AC5-29995). Additional support was received from MSE Technology Applications, Inc. (Butte, MT) in form of a scholarship for K. Johnson as part of the Undergraduate Women in Environmental Engineering Research Program at the University of Iowa. We also wish to thank Richard L. Valentine (University of Iowa) for his valuable discussions on mass transport, Craig L. Just (University of Iowa) for his assistance with HPLC analysis, and Martin St. Clair (Coe College) for his insightful comments on the manuscript.

Nomenclature

b_x	Tafel slope for reaction x, V
C^s	aqueous surface concentration of reactant, mol cm^{-3}
C^b	aqueous bulk concentration of reactant, mol cm^{-3}
d	particle diameter, mm
D	molecular diffusion coefficient, cm^2 s^{-1}
D_{a1}	first Damköhler number
D_{a2}	second Damköhler number
E	electrode potential relative to a standard reference electrode, V
E_x^{eq}	Nernst equilibrium potential for reaction x, V

E_{corr}	corrosion potential (where net current is equal to zero), V
f	revolutions per second, rev s^{-1}
F	Faraday's constant ($F = 96485$ C mol^{-1})
j_{net}	net observed current density, A cm^{-2}
j_x	overall partial current density for reaction x, A cm^{-2}
$j_{x,rxn}$	partial current density for reaction x, A cm^{-2}
$j_{x,mt}$	partial current density for mass transport of species x, A cm^{-2}
j_x^0	exchange current density for reaction x, A cm^{-2}
k_x^0	standard heterogeneous reaction rate coefficient, cm s^{-1}
k_{rxn}	first-order heterogeneous reaction rate coefficient, cm s^{-1}
k_{mt}	mass transport rate coefficient, cm s^{-1}
k_{SA}	BET surface area normalized heterogeneous reaction rate coefficient, L m^{-2} h^{-1}
$k_{overall}$	surface area normalized overall rate coefficient, cm s^{-1} or L m^{-2} h^{-1}
n	number of electrons
N	amount of product, mol
q	amount of charge, C
Re	Reynolds number
Sh	Sherwood number
Sc	Schmidt number
ϵ	porosity
τ_{RH}	hydraulic residence time, s
u	fluid velocity, m dy^{-1}
ν	kinematic viscosity, cm^2 s^{-1}
ω	angular velocity of RDE, s^{-1}
Ω	external effectiveness factor

Supporting Information Available

A comparison of experimentally measured currents with estimated currents from eq 15 is shown. Linear regression of the data gives a slope of 1.05 ± 0.01 ($R^2 = 0.99$) which is reasonably close to the theoretical slope of 1 for perfect agreement between the estimated currents and experimentally measured currents. This material is available free of charge via the Internet at http://pubs.acs.org.

Literature Cited

(1) Powell, R. M.; Puls, R. W.; Blowes, D. W.; Vogan, J. L.; Gillham, R. W.; Powell, P. D.; Schultz, D.; Landis, R.; Sivavec, T. *Permeable Reactive Barrier Technologies for Contaminant Remediation*; EPA/600/R-98/125; U.S. Environmental Protection Agency: 1998.

(2) Lackovic, J. A.; Nikolaidis, N. P.; Dobbs, G. M. *Environ. Eng. Sci.* **2000**, *17*, 29−39.

(3) Puls, R. W.; Paul, C. J.; Powell, R. M. *Appl. Geochem.* **1999**, *14*, 989−1000.

(4) Pratt, A. R.; Blowes, D. W.; Ptacek, C. J. *Environ. Sci. Technol.* **1997**, *31*, 2492.

(5) Cantrell, K. J.; Kaplan, D. I.; Wietsma, T. W. *J. Haz. Mater.* **1995**, *42*, 201−212.

(6) Del Cul, G. D.; Bostick, W. D.; Trotter, D. R.; Osborne, P. E. *Sep. Sci. Technol.* **1993**, *28*, 551−564.

(7) Farrell, J.; Bostick, W. D.; Jarabek, R. J.; Fiedor, J. N. *Ground Water* **1999**, *37*, 618−4.

(8) Singh, J.; Shea, P. J.; Hundal, L. S.; Comfort, S. D.; Zhang, T. C.; Hage, D. S. *Weed Sci.* **1998**, *46*, 381−388.

(9) Sayles, G. D.; You, G. R.; Wang, M. X.; Kupferle, M. J. *Environ. Sci. Technol.* **1997**, *31*, 3448−3454.

(10) Eykholt, G. R.; Davenport, D. T. *Environ. Sci. Technol.* **1998**, *32*, 1482−1487.

(11) Nam, S.; Tratnyek, P. G. *Water Res.* **2000**, *34*, 1837−1845.

(12) Weber, E. J. *Environ. Sci. Technol.* **1996**, *30*, 716−719.

(13) Hung, H. M.; Ling, F. H.; Hoffmann, M. R. *Environ. Sci. Technol.* **2000**, *34*, 1758−1763.

(14) Singh, J.; Comfort, S. D.; Shea, P. J. *Environ. Sci. Technol.* **1999**, *33*, 1488−1494.

(15) Singh, J.; Comfort, S. D.; Shea, P. J. *J. Environ. Qual* **1998**, *27*, 1240−1245.

(16) Devlin, J. F.; Klausen, J.; Schwarzenbach, R. P. *Environ. Sci. Technol.* **1998**, *32*, 1941−1947.

(17) Agrawal, A.; Tratnyek, P. G. *Environ. Sci. Technol.* **1996**, *30*, 153−160.

(18) Hundal, L. S.; Singh, J.; Bier, E. L.; Shea, P. J.; Comfort, S. D.; Powers, W. L. *Environ. Pollut.* **1997**, *97*, 55−64.

(19) Arnold, W. A.; Ball, W. P.; Roberts, A. L. *J. Contam. Hydrol.* **1999**, *40*, 183−200.

(20) Burris, D. R.; Allen-King, R. M.; Manoranjan, V. S.; Campbell, T. J.; Loraine, G. A.; Deng, B. *J. Environ. Eng.* **1998**, *124*, 1012−1019.

(21) Scherer, M. M.; Westall, J. C.; Ziomek-Moroz, M.; Tratnyek, P. G. *Environ. Sci. Technol.* **1997**, *31*, 2385−2391.

(22) Burris, D. R.; Hatfield, K.; Wolfe, N. L. *J. Environ. Eng., ASCE* **1996**, *122*, 685−691.

(23) Johnson, T. L.; Scherer, M. M.; Tratnyek, P. G. *Environ. Sci. Technol.* **1996**, *30*, 2634−2640.

(24) Scherer, M. M.; Balko, B. A.; Tratnyek, P. G. The role of oxides in reduction reactions at the metal-water interface. In *Mineral Water Interfacial Reactions: Kinetics and Mechanisms*; Sparks, D., Grundl, T., Eds.; ACS Symposium Series No. 715; American Chemical Society: Washington, DC, 1998; pp 301−322.

(25) Riddiford, A. C. *The rotating disk system*; Delahay, P., Ed.; Wiley: New York, 1966; pp 47−111.

(26) Levich, V. G. *Physicochemical Hydrodynamics*; Prentice-Hall: Englewood Cliffs, NJ, 1962.

(27) Farrell, J.; Melitas, N.; Kason, M.; Li, T. *Environ. Sci. Technol.* **2000**, *34*, 2549−2556.

(28) Farrell, J.; Kason, M.; Melitas, N.; Li, T. *Environ. Sci. Technol.* **2000**, *34*, 514−521.

(29) Li, T.; Farrell, J. *Environ. Sci. Technol.* **2000**, *34*, 173−179.

(30) Liu, Z.; Arnold, R. G.; Betterton, E. A.; Festa, K. D. *Environ. Eng. Sci.* **1999**, *16*, 1−13.

(31) Bard, A. J.; Faulkner, L. R. *Electrochemical Methods. Fundamentals and Applications*; Wiley: New York, 1980.

(32) Klausen, J.; Trüber, S. P.; Haderlein, S. B.; Schwarzenbach, R. P. *Environ. Sci. Technol.* **1995**, *29*, 2396−2404.

(33) Shindo, H.; Nishihara, C. *J. Electroanal. Chem.* **1989**, *263*, 415−420.

(34) Wilke, C. R.; Chang, P. *A. I. Ch. E. J.* **1955**, *1*, 264−270.

(35) Cussler, E. L. *Diffusion Mass Transfer in Fluid Systems*, 2nd ed.; Cambridge University Press: New York, 1997.

(36) Roberts, P. V.; Cornel, P.; Summers, S. R. *J. Environ. Eng., ASCE* **1985**, *111*, 891−905.

(37) Wilson, E. J.; Geankoplis, C. J. *I&EC Fundam.* **1966**, *5*, 9−14.

(38) Mackenzie, P. D.; Horney, D. P.; Sivavec, T. M. *J. Haz. Mater.* **1999**, *68*, 1−17.

(39) Fogler, S. H. *Elements of Chemical Reaction Engineering*, 2nd ed.; Prentice Hall: Englewood Cliffs, NJ, 1992.

(40) Ramaswami, A.; Luthy, R. *Environ. Sci. Technol.* **1997**, *31*, 2260−2267.

(41) Khandelwal, A.; Rabideau, A. J. *Water Res. Res.* **1999**, *35*, 1939−1945.

(42) Hatfield, K.; Burris, D. R.; Wolfe, N. L. *J. Environ. Eng., ASCE* **1996**, *122*, 676−684.

(43) Eykholt, G. R.; Sivavec, T. M. Contaminant transport issues for reactive-permeable barriers. In *Geoenvironment 2000, Characterization, containment, remediation, and performance in environmental geotechnics*; Acar, Y. B., Daniel, D. E., Eds.; American Society of Civil Engineers: New York, 1995; Vol. 2, pp 1608−1621.

(44) Tratnyek, P. G.; Johnson, T. L.; Scherer, M. M.; Eykholt, G. R. *Ground Water Monit. Rem.* **1997**, 108−114.
(45) Eykholt, G. R. *Uncertainty-based scaling of iron reactive barriers*; Evans, J., Reddi, L., Eds.; American Society of Civil Engineers: New York, 1997; pp 41−55.
(46) Haderlein, S. B.; Schwarzenbach, R. P. Environmental processes influencing the rate of abiotic reduction of nitroaromatic compounds in the subsurface. In *Biodegradation of Nitroaromatic Compounds*; Spain, J. C., Ed.; Plenum: New York, 1995; pp 199−225.

Received for review September 20, 2000. Revised manuscript received April 6, 2001. Accepted April 6, 2001.

ES0016856